Available online at www.sciencedirect.com
ScienceDirect
Geochimica et Cosmochimica Acta 73 (2009) 1095–1108
Geochimica et Cosmochimica Acta
www.elsevier.com/locate/gca

LA-MC-ICPMS and SHRIMP U–Pb dating of complex zircons from Quaternary tephras from the French Massif Central: Magma residence time and geochemical implications

Alain Cocherie [a,*], C. Mark Fanning [b], Pierre Jezequel [a], Michèle Robert [a]

[a] *BRGM, BP 36009, 45060 Orléans Cedex 2, France*
[b] *Research School of Earth Sciences, ANU, Canberra, ACT 0200, Australia*

Received 3 July 2008; accepted in revised form 18 November 2008; available online 6 December 2008

Abstract

Analyses of zircon grains from the Queureuilh Quaternary tephras (pumice) provide new information about their pre-eruptive history. U–Pb dating was performed *in situ* using two methods: SHRIMP and LA-MC-ICPMS equipped with a multi-ion counting system. Both methods provided reliable $^{207}Pb/^{206}Pb$ and $^{206}Pb/^{238}U$ ratios as well as U and Th abundances required for U–Pb Concordia intercept age determination, after initial ^{230}Th disequilibrium correction. The new LA-MC-ICPMS method was validated by dating a reference zircon (61.308B) and zircons from a phonolitic lava dated independently with the two techniques. A time resolution of about 20 kyr for 1 Ma zircon crystals was achieved for both methods.

The clear euhedral zircon population from Queureuilh tephras is quite complex from several points of view: (1) some grains are reddish or yellowish while others are colorless; (2) the U and Th composition changes by more than an order of magnitude and Th/U is generally high (~1–2); (3) there are three discrete ages recorded at 2.35 ± 0.04, 1.017 ± 0.008 and 0.640 ± 0.010 Ma.

From the previously determined $^{40}Ar/^{39}Ar$ age at 0.571 ± 0.060 Ma [Duffell H. (1999) Contribution géochronologique à la stratigraphie volcanique du Massif des Monts Dore par la méthode $^{40}Ar/^{39}Ar$. D.E.A. Univ. Clermont-Ferrand, 56 p.], the discontinuous zircon age populations, the color of the grains and their composition, we favor the following model as explanation: The oldest, less numerous group of reddish zircons represents xenocrystic grains resulting from assimilation of the local material during magma ascent. A primitive magma chamber, perhaps deep in crustal level, was formed at 1.0 Ma. The related magma, previously characterized by high Th/U ratio (2.2 ± 1.1), underwent rejuvenation during ascent to a new chamber at shallow depth and/or during injection of more mafic magmas. During this stage, at 0.64 Ma, the colorless zircon grains of lower Th/U ratio (1.3 ± 0.5) crystallized. This last stage defined the magma residence time of 70 kyr prior to eruption dated by the $^{40}Ar/^{39}Ar$ method. However, if the primitive magma is considered, the magma residence time as a whole from this first stage reached 446 kyr.

In the light of the complex history of such magmas, which commonly involves recycling of zircon grains that precipitated tens to hundreds of kyr earlier than eruptions, the use of Zr concentration in geochemical modeling of whole rock compositional data can be problematic.

1. INTRODUCTION

Tephra or ash layers are marker beds that allow correlation of stratigraphic sequences between various locations by providing precise chronostratigraphic points (Alloway et al., 2006). They provide very useful chronological control for a wide range of disciplines from archaeological reconstructions to volcanic history. Zircon is a remarkably robust mineral, which commonly is observed in tephras of rhyolitic composition. It generally forms a closed reservoir for radiogenic Pb even when subject to intense and

* Corresponding author.
E-mail address: a.cocherie@brgm.fr (A. Cocherie).

0016-7037/$ - see front matter © 2008 Elsevier Ltd. All rights reserved.
doi:10.1016/j.gca.2008.11.028

prolonged heating. However, there are a number of complications such as zircon may suffer partial resetting due to cumulative lattice damage resulting from α-recoil in U rich parts, especially when associated with fluid interaction (Balan et al., 2001). As the extent of the subsequent metamictization process is also a function time, young Quaternary zircons are not likely to be altered even when the U content reaches 1000 ppm or more (Cherniak and Watson, 2000). The second commonly cited drawback of the U–Pb zircon method is that inherited grains or cores are frequently observed due to either incomplete fusion of an initial crustal source or from direct crustal contamination (e.g. inherited from the source or from the wall rocks). The third drawback is related to common-Pb contribution, which can easily be subtracted by measuring ^{204}Pb when dating Proterozoic zircons or those rich in radiogenic Pb. In contrast, due to the very low level of the $^{206}Pb^{*}$ (radiogenic) in Quaternary zircon, common-Pb corrections are difficult due to the large uncertainty of measured $^{206}Pb/^{204}Pb$ and uncertainties in common-Pb composition. To avoid the issue of common-Pb correction it is more suitable to analyze restricted subgrain domains free of any defects or inclusions that contain potentially high common-Pb levels keeping in mind that common-Pb can also be in the structure of the grain itself. The Tera and Wasserburg (1972) Concordia diagram is used for such young zircon analyses, firstly because it allows the data to be plotted without preliminary common-Pb correction. Secondly because it has the significant advantage that young zircons have almost invariant $^{207}Pb^{*}/^{206}Pb^{*}$ ratios and the Concordia is thus near-parallel to the abscissa making the common-Pb proportion and radiogenic $^{206}Pb/^{238}U$ intercept easy to calculate. At the very least, care must be taken to minimize common-Pb contamination during sample preparation, especially by avoiding any chemical preparation that would lead to significant common-Pb contamination. Due to all these reasons, it is of great interest to perform direct *in situ* measurements at the best spatial resolution (e.g. about 20 μm). Until now, the unique isotopic method providing sensitive *in situ* measurements involving almost no common-Pb contamination associated with the analyses was by ion microprobe (e.g. CAMECA 1270, Schmitt et al., 2003; or SHRIMP, see Compston et al., 1982). It has been demonstrated that zircon as young as 1 Ma and even less can also be dated (for instance, Brown and Fletcher, 1999; Bacon et al., 2000; Vazquez et al. 2007 have given reliable ages of about 340, 100 and 300 ka, respectively). Recently, an alternative method has emerged that employs MC-ICPMS (Multi Collector Inductively Coupled Plasma Mass Spectrometer) together with laser ablation (Cocherie et al., 2007; Cocherie and Robert, 2008). Significantly, a multi-ion counting system (MIC) allows high sensitivity and precision to be achieved for such transient signals.

The aim of this work is to demonstrate the ability of the LA-MC-ICPMS technique to allow reliable U–Pb geochronology applied to Quaternary zircon to be performed analyzing a crater of 20 μm in diameter (~18 μm deep). As a comparison, a laser crater provides a volume of analyzed material about 10 times larger than that extracted by the primary beam of the SHRIMP (spot size of 20 μm with 1–2 μm depth). Firstly, a 2 Ma reference zircon 61.308B (Wiedenbeck et al., 1995) was dated using LA-MC-ICPMS alone, and secondly, zircon grains from the Sanadoire phonolite collected in the Monts Dore Massif (French Massif Central) were dated using both SHRIMP and LA-MC-ICPMS techniques. Following on from the demonstrated ability, both techniques were applied to the more complicated zircon populations in Queureuilh trachytic ash and pumice flow from the Monts Dore Massif, whose emplacement has previously been dated at 0.571 ± 0.060 Ma using $^{40}Ar/^{39}Ar$ on feldspars (Duffell, 1999). These results provide an opportunity to evaluate the significance of calculated Zr partition coefficients between any phases and the glass in equilibrium when zircon crystals of various origins remain in a melt. They also provide information on the pre-eruptive magma history and enable an estimation of the magma residence time. Contrasting histories of crystallization and melt evolution have been reported, frequently comparing zircon crystallization (U–Pb or $^{230}Th–^{238}U$ disequilibrium) and feldspar crystallization ($^{40}Ar/^{39}Ar$). The possibility of miscalibration of the ^{40}Ar decay constants has even been considered (Palfy et al., 2007; Simon et al., 2008). The conclusions of such studies are highly contrasting: Condomines (1997) calculated a very short time interval (~1 kyr) between crystallization of zircon and eruption of a small volume of trachytic magma while Oberli et al. (2004) demonstrated an extended history of crystallization and tonalitic melt evolution of at least 5 Myr. Similarly, U–Pb zircon dating from the Cretaceous Tuolumne and Mt. Stuart batholiths has shown that the timeframe of pluton assembly is considerable: >5 Myr and even >8 Myr for Tuolumne (Miller et al., 2007). To achieve a better understanding of the extent of crystallization history, Bachmann et al. (2007a) determined highly precise and accurate U–Pb and $^{40}Ar/^{39}Ar$ ages on minerals extracted from a 28 Ma old volcanic system. In the light of these previous studies, we consider that dating recent Quaternary events should lead to more precise knowledge of the complex crystallization processes in magmatic chambers (e.g. see Bacon and Lowenstern, 2005; Bachmann et al., 2007b; Simon et al., 2008 and references therein).

2. GEOLOGICAL SETTING

The Monts Dore Massif is located in the northern part of the French Massif Central volcanic area. It lies between the Mio-Pliocene volcanism of Cézallier to the south (e.g. the Sancy stratovolcano) and the Quaternary volcanism of the Chaîne des Puys to the north. (e.g. the Monts Dore stratovolcano). The massif covers an area of around 500 km^2, while the volume of volcanic products has been estimated at around 70 km^3 (Baubron and Cantagrel, 1980; Cantagrel and Baubron, 1983). The Monts Dore Massif has been built on a Variscan basement previously covered by alkalic volcanics during Miocene–Pliocene times. The volcanic pile comprises two volcanoes: between 2.5 and 1.6 Ma the northern volcanic centers were formed and from 0.9 to 0.25 Ma the Sancy volcano was active. At 2 Ma episodic undersaturated volcanism to which the Sanadoire phonolite belongs was superimposed (Baubron and Cantagrel, 1980).

3. ANALYTICAL PROCEDURE

3.1. SHRIMP

The Sensitive High mass Resolution Ion MicroProbe (SHRIMP) was specifically built for geological applications, including U–Pb geochronology. For this current study, zircon grains were separated from total rock using standard mineral separation procedures and then mounted in epoxy together with chips of reference zircons: TEMORA (Black et al., 2003) and SL13, sectioned approximately in half, and polished. Reflected and transmitted light photomicrographs were prepared for all zircons, as were cathodoluminescence (CL) Scanning Electron Microscope (SEM) images. These CL images were used to decipher the internal structures of the sectioned grains and to ensure that the ~20 μm SHRIMP spot was wholly within a single age component within the sectioned grains.

The U–Th–Pb analyses were made using SHRIMP II at the Research School of Earth Sciences, The Australian National University, Canberra, Australia following procedures given in Williams (1998, and references therein). Each analysis consisted of six scans through the mass range, with the TEMORA reference zircon grains analyzed for every three unknown analyses. The data have been reduced using the SQUID Excel Macro of Ludwig (2001). The Pb/U ratios have been normalized relative to a value of 0.0668 for the TEMORA reference zircon, equivalent to an age of 417 Ma (see Black et al., 2003). Uncertainty in U–Pb calibration was 0.29%, 0.55% and 0.32% for the three SHRIMP II sessions: Sanadoire, Queureuilh 1 and 2, respectively.

Uncertainties given in the tables for individual analyses (ratios and ages) are at 1σ level. Tera and Wasserburg (1972) Concordia plots, probability density plot with stacked histograms and weighted mean $^{206}Pb/^{238}U$ ages calculations were carried out using Isopot/EX (Ludwig, 2003). These calculations and uncertainties are reported as 95% confidence limits.

3.2. LA-MC-ICPMS

Improvements in the technology of laser ablation and ICPMS instruments make LA-MC-ICPMS a rapid, precise and accurate method for U–Pb zircon geochronology. The development of magnetic sector field instruments equipped with an electrostatic analyzer enables for double focusing and thus flat peak tops required for precise isotopic ratio measurement. Reliable geochronology can now be performed with such instrumentation (e.g. Willigers et al., 2002; Horstwood et al. 2003; Tiepolo, 2003; Hirata et al, 2005; Paul et al., 2005; Simonetti et al., 2005). More recently, Cocherie and Robert (2008) demonstrated that by combining a 213 nm UV laser and a MC-ICPMS (Neptune, ThermoFisherScientific) equipped with a multi-ion counting system (MIC) operating in static mode, all masses of interest can be simultaneously recorded (^{202}Hg, ^{204}Pb, ^{206}Pb, ^{207}Pb, ^{208}Pb on ion counters, and ^{232}Th and ^{238}U on Faraday cup collectors). The detailed analytical procedure presented in Cocherie and Robert (2008) and is summarized below, with the details of specific adaptations necessary to date very young zircons. As shown in the application of the MIC system for Pb isotopic ratio measurements in environmental sample solutions, e.g. rainwater (Cocherie and Robert, 2007), a sample-standard bracketing technique has to be applied to correct for the slight change in ion counter yields during an analytical session. This is required for all ratios and especially for the $^{207}Pb/^{206}Pb$ and $^{206}Pb/^{238}U$ ratios. After blank subtraction, the raw value of each sample was used for the calculation of isotope ratio, uncorrected for common-Pb. The $^{207}Pb/^{206}Pb$ and $^{206}Pb/^{238}U$ ratios were normalized using the average of the two analyses of the 91,500 standard zircon before and after, according to the following sequence: blank1, Sdr1, blank2, sample1, sample2, blank3, Sdr2, blank4, sample3, sample4, blank5, Sdr3, blank6, etc. The same counting time of 90 s was applied for blanks, samples and standards. The mass bias, the shift of the yield of the ion counters during the analytical session, the shift of the ion counter *vs.* Faraday cup calibration and the elemental fractionation due to laser ablation were all satisfactorily corrected using the 91,500 zircon standard (Cocherie and Robert, 2008). Taking into account the time to return to background level between each analysis, the duration for a typical age determination including 22 spot analyses on unknown grains was 3 h. He gas was not added as tests showed that it did not enhance of the Pb signal nor result in an improvement of the signal/blank ratio. The common in-run precisions achieved for the key ratios $^{207}Pb/^{206}Pb$ and $^{206}Pb/^{238}U$ were better than 1% and 3% (2σ), respectively, including error propagation associated with standard normalization and blank subtraction. These precisions were obtained from a single crater (20 μm in diameter and ~18 μm in depth) and are regarded as actual *in situ* measurements within a single zircon grain (Fig. 1). In general, the analysis of 16–20 spot gives a $^{206}Pb/^{238}U$ age uncertainty of between 3 to 7 Ma from testing four zircon samples covering a wide age range of 290–2440 Ma (Cocherie and Robert, 2008).

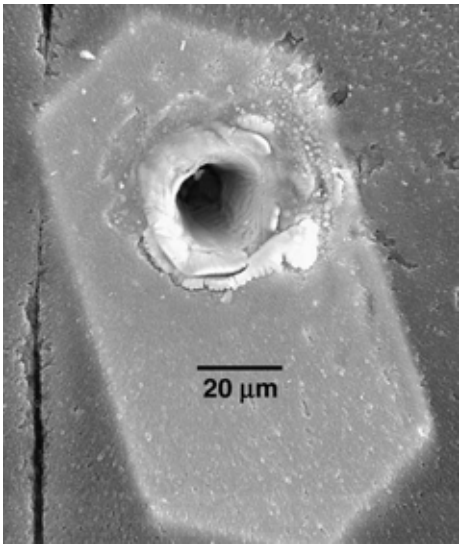

Fig. 1. Secondary electron image of the crater obtained after a laser shot of 92 s (Nd:YAG, 213 nm UV) on a zircon grain.

For Quaternary zircon, the energy of the laser beam was enhanced (laser beam energy enhanced from 0.3 to 1.5 mJ/pulse) which increased the sensitivity by a factor of 4. In such conditions, the count rate increased from 20,000 up to 80,000 cps for the ^{206}Pb peak of the reference zircon standard 91,500 (14.8 ppm Pb, Wiedenbeck et al., 1995). Traditionally, the SIMS community has empirically calculated the "useful yield" (ions detected *vs.* atoms removed from the crater, see Hervig et al., 2006). This parameter describes the sensitivity of destructive microanalytical techniques, e.g. SHRIMP useful yield is about 1% (Compston, 1999). It can also be useful to characterize the effect of the size and the energy of the laser beam on the ion yields for Pb and U respectively. When switching from low energy to high energy, the size of the crater slightly increases from 20 to 24 μm in diameter while it remains the same in depth (~18 μm) for the 90 s analytical data. Consequently, the amount of removed material is increased by a factor of 1.44. Considering the effective time of data collection (60 s) and the change from low to high energy, the useful yield increased by a factor of 2.78 for Pb, from 8.89E−4 to 2.47E−3 and only by a factor of 1.62 for U, from 1.68E−3 to 2.73E−3. The $^{207}Pb/^{206}Pb$ ratio remained quite constant during almost all of the 90 s of recording time. Usually, the period of effective data collection time taken into account is limited to about 60 s when the signal is high and the fractionation is low. Note that a pre-ablation stage (~10 s), included in the 90 s, is not used for isotopic ratio measurements. It allows any surface contamination to be avoided and a stable signal achieved. In contrast, the $^{206}Pb/^{238}U$ ratio changed regularly towards the end of the ablation time, as is the normally expected Pb/U fractionation associated with laser ablation. This observed fractionation is also affected by the fact that the laser beam is progressively defocused as the crater becomes deeper and deeper. According to Hirata's (1997) soft ablation technique, this trend can be significantly reduced by initially applying a slight defocusing of the laser beam (see Fig. 2a and b). Using this procedure, the statistical errors on $^{207}Pb/^{206}Pb$ and $^{206}Pb/^{238}U$ ratios (2σ level) for a 0.6 Ma old zircon containing 0.011 ppm $^{206}Pb^*$ and 147 ppm U are better than 4% and 3%, respectively (before blank subtraction; see Fig. 3a and b). Obviously, the blank from the gas needs to be as low as possible. The count rates of the blank were negligible for U and about 60–70 cps for ^{206}Pb. The analytical uncertainty on $^{206}Pb/^{238}U$ ages (including error on the blank) under these conditions re-

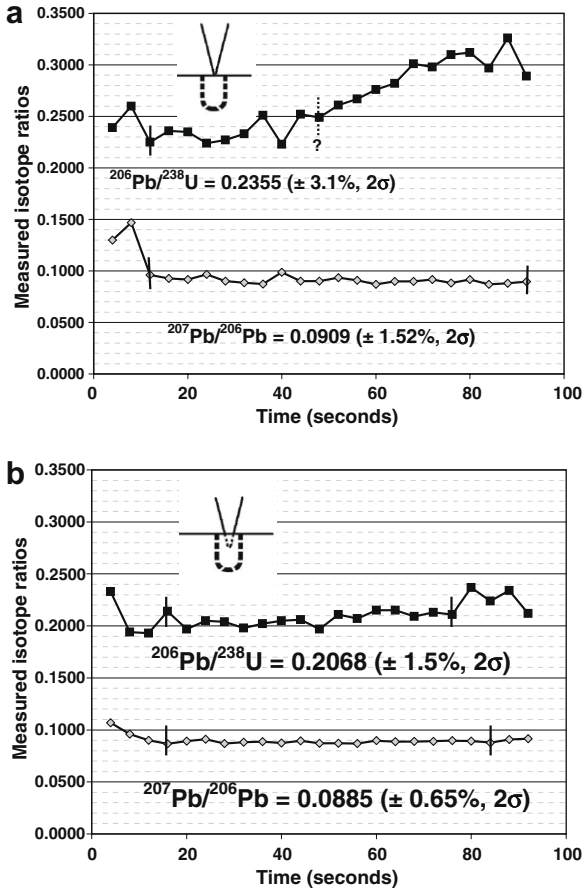

Fig. 2. (a) Typical block of 23 cycles recorded during a 92 s ablation time, the laser beam being focused on the surface of the grain (uncorrected raw data from the zircon standard 91,500). The second part of the recorded data shows a significant increase in the $^{206}Pb/^{238}U$ ratio. (b) Typical block of 23 cycles recorded during a 92 s ablation time, applying a slight defocusing of the laser beam (uncorrected raw data from the zircon standard 91,500). Both isotope ratios remain quite constant throughout the ablation time, providing much better statistical precision: 1.5% and 0.65% for $^{206}Pb/^{238}U$ and $^{207}Pb/^{206}Pb$, respectively. The two bars to the symbols represent the first and last runs between which the average ratio was calculated.

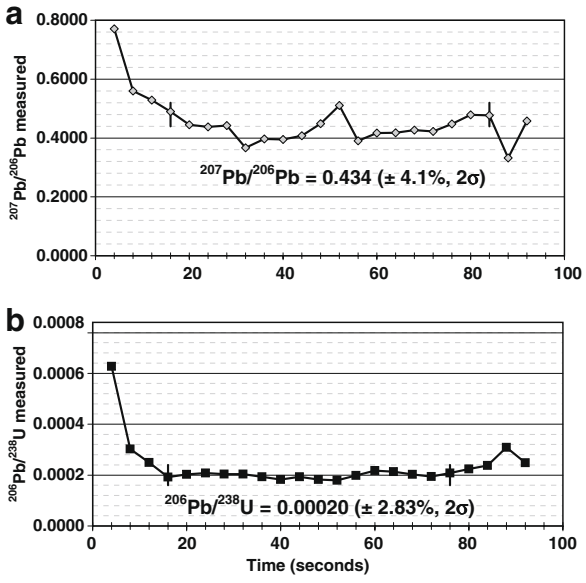

Fig. 3. (a) Uncorrected raw $^{207}Pb/^{206}Pb$ ratio (before blank subtraction) recorded for a typical zircon grain (spot 11.1) from Queureuilh pumice containing 11 ppb of $^{206}Pb^*$ and 147 ppm of U. (b) $^{206}Pb/^{238}U$ ratio for the same spot analysis. Note in both diagrams that an excess of $^{207}Pb/^{206}Pb$ and ^{206}Pb can be observed. This is not related to surface contamination, but to a larger contribution of the blank from the gas, just before the arrival of the ablated material itself in the mass spectrometer.

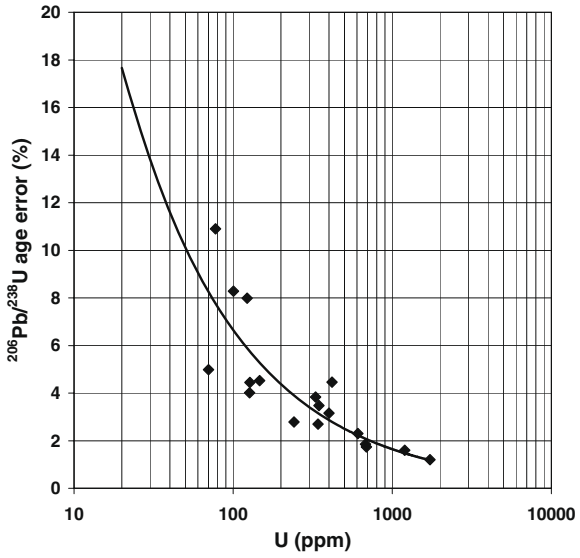

Fig. 4. Plot of $^{206}Pb/^{238}U$ age error as a function of U concentration for zircons dated in the range of 0.6–1.0 Ma using LA-MC-ICPMS (individual spots). A precision better than 5% can be achieved for U content >150 ppm.

mains better than 5% (2σ) for 0.6–1.0 Ma zircons containing more than 150 ppm U (Fig. 4).

Throughout, calculated uncertainties are given at the 2σ level (95% confidence limit) as determined by the ISOPLOT Excel macro of Ludwig (2003). The MSWD (Mean Square Weighted Deviation) parameter is used as a statistical test of validity of the regression line according to the criteria defined by Wendt and Carl (1991).

3.3. U–Pb age calculation for young zircons

Application of the Tera and Wasserburg (1972) Concordia plot enables Phanerozoic U–Pb ages to be visualized and calculated (see Claoué-Long et al., 1995; Williams, 1998). In Miocene to Pleistocene times, a significant change in age induces almost no variation in the $^{207}Pb^*/^{206}Pb^*$ ratio (Pb^*: radiogenic Pb), but considerable change in the $^{206}Pb^*/^{238}U$ ratio. The principles of the use of the Tera and Wasserburg Concordia diagram are that (1) unlike the conventional Concordia diagram it has the advantage that the x- and y-axis values show very little error correlation, (2) U–Pb data, which are not corrected for common-Pb, plot on a mixing line defined by the point on the Concordia and a point on the ordinate corresponding to the $^{207}Pb/^{206}Pb$ ratio of the common-Pb component at the time of zircon crystallization (Cumming and Richards, 1975). The crystallization age is given by the intercept of this line with the Concordia curve.

However, prior to calculating common-Pb corrected ages, the ^{230}Th disequilibrium needs to be considered, and the raw data corrected (Schärer, 1984), as this disequilibrium induces a deficit in ^{206}Pb for mineral phases showing Th/U ratio <1 such as zircon. To do so, the $^{232}Th/^{238}U$ ratio must be measured in the zircon itself and the Th/U ratio of the magma from which the zircon precipitated is also required. Considering that zircon mineral usually shows $f < 1$ ($f = (Th/U)_{mineral}/(Th/U)_{magma}$), the extent of the effect of ^{230}Th disequilibrium on the corrected ages is a function of two factors: the lower the f factor and the younger the grain, the higher the age correction (in relative notation).

$$^{206}Pb^* = {}^{238}U\{[EXP(\lambda_{238}T) - 1] + (\lambda_{238}/\lambda_{230}).(f - 1)\}$$

where $\lambda_{238} = 1.55125 \times 10^{-10}\,an^{-1}$ and $\lambda_{230} = 0.922 \times 10^{-5}\,an^{-1}$.

3.4. LA-MC-ICPMS results applied to young reference zircons

Two young reference zircons already dated by conventional U–Pb techniques were analyzed to check the accuracy of LA-MC-ICPMS: standard zircon 61.308B dated by three independent laboratories using conventional isotope dilution and thermal ionization mass spectrometry (ID-TIMS) and a reference zircon dated by SHRIMP II (ANU, Canberra).

3.4.1. Standard zircon 61.308B

This reference zircon (Wiedenbeck et al., 1995) from CNRS-CRPG (Nancy) was provided by the Muséum National d'Histoire Naturelle in Paris. The original crystal has a single well developed prism and a single well developed pyramid termination. It was collected originally from a deposit at Croustet, Haute Loire region, France, but the rock type from which it was derived is unknown. This zircon has a ID-TIMS weighted mean $^{206}Pb/^{238}U$ age of 2.508 ± 0.002 Ma. Unfortunately, the ^{230}Th disequilibrium effect cannot be corrected, because the composition of the original magma is unknown (LA-MC-ICPMS data, Table 1). Note that the $^{207}Pb/^{206}Pb$ ratio of 0.0339 measured for spot 1.1 (below 0.046, Table 1) must be interpreted as an analytical artefact. Our results can be directly compared with the reference value, both being uncorrected. An initial common $^{207}Pb/^{206}Pb$ ratio of 0.832 ± 0.002 has been assumed (Cumming and Richards, 1975). The calculated regression line upper intercept is fixed at 0.832 and passes through the data uncorrected for common-Pb to give a Concordia intercept at 2.510 ± 0.046 Ma (MSWD = 1.90). This is indistinguishable from the conventionally determined $^{206}Pb/^{238}U$ age within measurement uncertainties (Fig. 5). Note that the normalizing standard used was the 91,500 reference zircon, previously demonstrated to be suitable for zircons from Variscan to Archean times (Cocherie and Robert, 2008), and also suitable for very young zircons. The MSWD for all 12 analyses is 1.90, which is very close to the maximum value defined at 1.89 according to Wendt and Carl's (1991) calculations for 95% probability. For n points, the calculated linear regression has $(n - 2)$ degrees of freedom (f). Thus, to consider the 12 points as representative of a single population, the MSWD must be $< 1 + 2(2/f)^{1/2}$, with $f = 10$, MSWD < 1.89. In other words it means that our error calculation covers the real uncertainty on the age.

3.4.2. Sanadoire zircon (Monts Dore)

The emplacement age of the related phonolite lava has been estimated by Cantagrel and Baubron (1983) at around

Table 1
Summary of LA-MC-ICPMS U–Pb results for zircon standard 61.308B.

Grain spot	U (ppm)	Th (ppm)	Th/U	$^{206}Pb^{*}$ (ppm)	$^{206}Pb/^{204}Pb$	f_{206} %	Total				Radiogenic			Age (Ma)	
							$^{238}U/^{206}Pb$	±	$^{207}Pb/^{206}Pb$	±	$^{206}Pb/^{238}U$	±		$^{206}Pb/^{238}U$	±
Standard 61.308B (France)															
1.1	153	218	1.42	0.053	130	—	2527	63	0.0339	0.0021	0.000396	0.000010		2.550	0.064
1.2	157	210	1.34	0.054	131	2.42	2509	48	0.0651	0.0031	0.000389	0.000008		2.507	0.048
1.3	82	62	0.76	0.026	70	12.25	2326	58	0.1424	0.0077	0.000377	0.000009		2.432	0.060
1.4	256	428	1.67	0.086	—	—	2567	30	0.0414	0.0021	0.000390	0.000005		2.511	0.030
1.5	168	219	1.30	0.056	—	7.91	2395	35	0.1083	0.0058	0.000385	0.000006		2.479	0.036
1.6	105	105	1.01	0.035	—	1.93	2508	51	0.0613	0.0043	0.000391	0.000008		2.520	0.051
1.7	226	280	1.24	0.073	35	14.17	2278	62	0.1575	0.0085	0.000377	0.000010		2.429	0.066
1.8	58	46	0.79	0.018	97	—	2567	97	0.0451	0.0049	0.000390	0.000015		2.511	0.095
1.9	63	51	0.81	0.023	—	7.19	2187	65	0.1026	0.0097	0.000424	0.000013		2.735	0.081
1.10	97	86	0.89	0.032	20	18.91	2223	54	0.1948	0.0101	0.000365	0.000009		2.351	0.057
1.11	113	90	0.80	0.039	65	13.41	2097	69	0.1515	0.0079	0.000413	0.000014		2.662	0.088
1.12	204	258	1.26	0.068	194	7.04	2414	37	0.1015	0.0046	0.000385	0.000006		2.482	0.038

Notes: (1) Uncertainties given at the one σ level. (2) Error in 91,500 zircon reference standard is included in the above errors. (3) $^{206}Pb^{*}$: radiogenic ^{206}Pb. (4) f_{206}% denotes the percentage of ^{206}Pb that is common-Pb. (5) Correction for common-Pb made using the measured $^{238}U/^{206}Pb$ and $^{207}Pb/^{206}Pb$ ratios. Following Tera and Wasserburg (1972) as outlined in Williams (1998).

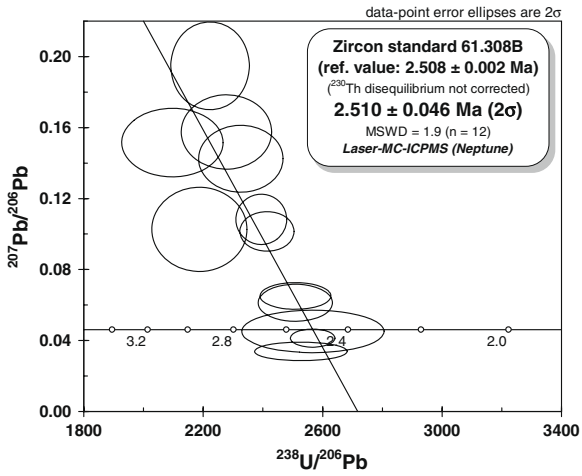

Fig. 5. Age determination for reference zircon standard 61.308B using the intercept of the common-Pb trend with the Concordia in the uncorrected Tera and Wasserburg diagram. The reference value and this new determination were not corrected for ^{230}Th disequilibrium, the host rock being unknown. The $^{207}Pb/^{206}Pb$ ratio of 0.0339 (Table 1) measured for spot 1.1 located below the Concordia curve corresponds to an analytical artefact in so far as it cannot be lower than 0.0460.

1.9–2.1 Ma using the K–Ar method. The main goal of our study was to compare the two *in situ* methods (LA-MC-ICPMS and SHRIMP) applied to such well formed euhedral zircon grains showing almost no defects or alteration (Fig. 6). A high Th/U ratio was measured on the whole rock (Th = 15 ppm and U = 1.5 ppm). Initial ^{230}Th disequilibrium was corrected (Schärer, 1984), using individually measured Th/U ratios for zircons and the Th/U ratio

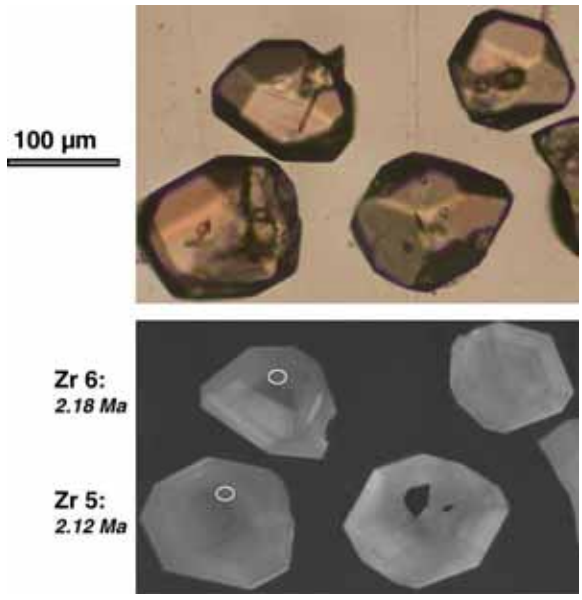

Fig. 6. Representative transmitted light and cathodoluminescence images of zircon grains from Sanadoire phonolite mounted in polished section and analyzed using SHRIMP II. Spots are visible on the post-analysis transmitted light image and they are also marked on the CL image.

Table 2
Summary of SHRIMP and LA-MC-ICPMS U–Pb results from Sanadoire phonolite. In italics, data not included in the average age of the zircons from a given rock sample.

Grain spot	U (ppm)	Th (ppm)	Th/U	$^{206}Pb^{*}$ (ppm)	$^{206}Pb/^{204}Pb$	f_{206} %	Total (U–Th desequil. corrected)				f Th/U	Radiogenic		Age (Ma)	
							$^{238}U/^{206}Pb$	±	$^{207}Pb/^{206}Pb$	±		$^{206}Pb/^{238}U$	±	$^{206}Pb/^{238}U$	±
LA-MC-ICPMS															
1.1	132	239	1.80	0.035	261	4.42	2916	73	0.0809	0.0122	0.144	0.000328	0.000008	2.113	0.053
2.1	141	270	1.92	0.038	49	6.04	2851	56	0.0936	0.0107	0.153	0.000330	0.000006	2.124	0.041
3.1	284	753	2.65	0.080	36	13.31	2576	65	0.1508	0.0068	0.212	0.000337	0.000009	2.169	0.055
4.1	*150*	*206*	*1.37*	*0.045*	—	—	*2628*	*44*	*0.0445*	*0.0079*	*0.110*	*0.000381*	*0.000006*	*2.453*	*0.041*
5.1	297	937	3.15	0.078	—	2.82	2983	56	0.0683	0.0057	0.252	0.000326	0.000006	2.100	0.039
6.1	*103*	*150*	*1.45*	*0.031*	—	*6.35*	*2377*	*50*	*0.0960*	*0.0116*	*0.116*	*0.000394*	*0.000008*	*2.539*	*0.053*
7.1	312	973	3.12	0.088	—	7.29	2854	42	0.1034	0.0056	0.250	0.000325	0.000005	2.094	0.031
8.1	215	506	2.36	0.054	—	2.67	3085	40	0.0671	0.0098	0.189	0.000315	0.000004	2.034	0.026
9.1	261	690	2.64	0.064	—	2.75	3017	47	0.0677	0.0051	0.212	0.000322	0.000005	2.078	0.033
11.1	414	1548	3.74	0.114	—	4.15	2871	40	0.0787	0.0039	0.299	0.000334	0.000005	2.152	0.030
11.2	533	1193	2.24	0.130	109	6.67	2773	39	0.0986	0.0034	0.179	0.000337	0.000005	2.169	0.031
12.1	723	2016	2.79	0.164	163	8.11	2814	42	0.1099	0.0067	0.223	0.000327	0.000005	2.105	0.031
13.1	*199*	*417*	*2.09*	*0.062*	—	—	*2619*	*32*	*0.0338*	*0.0050*	*0.168*	*0.000382*	*0.000005*	*2.461*	*0.030*
14.1	194	375	1.94	0.045	—	3.90	2873	68	0.0768	0.0050	0.155	0.000335	0.000008	2.156	0.051
16.1	283	803	2.83	0.073	64	3.89	2963	37	0.0766	0.0065	0.227	0.000324	0.000004	2.091	0.026
17.1	339	865	2.55	0.090	—	1.74	2906	37	0.0598	0.0051	0.204	0.000338	0.000004	2.179	0.027
18.1	76	85	1.12	0.019	31	10.68	2813	80	0.1301	0.0336	0.090	0.000318	0.000009	2.047	0.058
19.1	*219*	*518*	*2.37*	*0.060*	*33*	*4.64*	*2704*	*52*	*0.0826*	*0.0086*	*0.189*	*0.000353*	*0.000007*	*2.273*	*0.043*
20.1	*471*	*1553*	*3.29*	*0.131*	—	*5.55*	*2683*	*36*	*0.0897*	*0.0043*	*0.263*	*0.000352*	*0.000005*	*2.269*	*0.030*
21.1	235	469	2.00	0.062	—	4.54	2881	49	0.0818	0.0089	0.160	0.000331	0.000006	2.136	0.036
22.1	349	1053	3.02	0.080	138	1.36	3122	63	0.0568	0.0048	0.242	0.000316	0.000006	2.037	0.041
23.1	697	3175	4.56	0.201	—	0.66	2909	33	0.0513	0.0023	0.364	0.000341	0.000004	2.201	0.025
SHRIMP II															
1.1	*348*	*873*	*2.51*	*0.11*	*32*	*6.41*	*2592*	*87*	*0.0965*	*0.0090*	*0.201*	*0.000361*	*0.000012*	*2.328*	*0.078*
2.1	224	362	1.61	0.06	32	9.13	2861	124	0.1179	0.0145	0.129	0.000318	0.000014	2.047	0.091
3.1	*907*	*3887*	*4.28*	*0.27*	—	*2.95*	*2752*	*62*	*0.0693*	*0.0049*	*0.343*	*0.000353*	*0.000008*	*2.273*	*0.050*
4.1	428	927	2.16	0.12	—	5.74	2837	91	0.0912	0.0089	0.173	0.000332	0.000011	2.142	0.068
5.1	672	2183	3.25	0.19	224	2.45	2962	79	0.0654	0.0062	0.260	0.000329	0.000009	2.123	0.055
6.1	887	3022	3.41	0.25	—	2.28	2886	115	0.0640	0.0058	0.272	0.000339	0.000013	2.182	0.082
7.1	443	1043	2.35	0.13	53	6.99	2903	93	0.1011	0.0094	0.188	0.000320	0.000010	2.065	0.066
8.1	208	336	1.61	0.06	16	15.62	2834	124	0.1689	0.0168	0.129	0.000298	0.000014	1.919	0.090
9.1	226	411	1.81	0.07	59	9.91	2716	114	0.1240	0.0148	0.145	0.000332	0.000015	2.138	0.094
10.1	568	1473	2.59	0.16	165	5.19	3004	73	0.0869	0.0074	0.207	0.000316	0.000008	2.034	0.049
11.1	266	556	2.09	0.07	34	9.13	2977	100	0.1179	0.0123	0.167	0.000305	0.000011	1.968	0.069
12.1	583	2021	3.47	0.16	171	3.95	2969	71	0.0771	0.0071	0.278	0.000324	0.000008	2.085	0.050
13.1	1173	5691	4.85	0.33	465	3.11	2924	53	0.0705	0.0043	0.388	0.000331	0.000006	2.136	0.038
14.1	213	346	1.62	0.07	55	11.55	2647	95	0.1369	0.0166	0.130	0.000334	0.000014	2.153	0.087

Notes: (1) Uncertainties given at the one σ level. (2) Error in 91,500 zircon reference standard is included in the above errors (LA-MC-ICPMS). (3) Error in Temora reference zircon calibration was 0.29% for the SHRIMP session, included in above errors. (4) f_{206}% denotes the percentage of ^{206}Pb that is common-Pb. (5) Correction for common-Pb made using the measured $^{238}U/^{206}Pb$ and $^{207}Pb/^{206}Pb$ ratios. Following Tera and Wasserburg (1972) as outlined in Williams (1998). (6) $f_{Th/U}$ denotes the degree of Th–U fractionation between mineral and magma which is given by $f = (Th/U)_{mineral}/(Th/U)_{magma}$ for this phonolite, Th/U = 12.5. (7) In case of zircon, a correction for deficit in ^{206}Pb is required, due to a deficiency of ^{230}Th (Schärer, 1984).

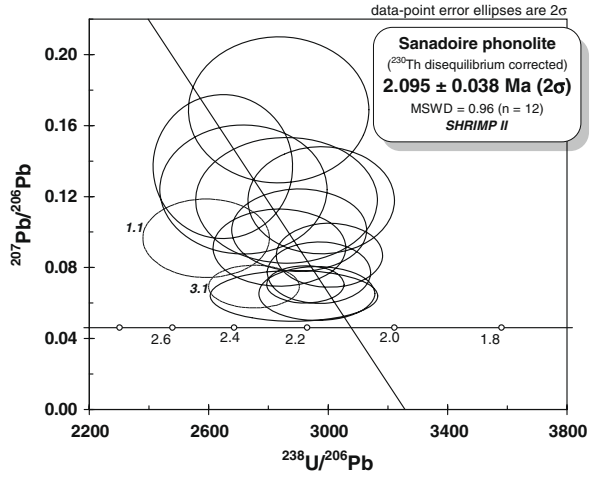

Fig. 7. Age determination for zircon from Sanadoire phonolite using SHRIMP II (corrected for ^{230}Th disequilibrium and common-Pb).

of the corresponding lava. The related f factor ($f = \mathrm{Th/U_{zircon}}/\mathrm{Th/U_{magma}}$) was calculated for each spot analysis and a ^{207}Pb/^{206}Pb ratio of 0.832 ± 0.002 was used for common-Pb correction.

Twenty-two spots were analyzed using LA-MC-ICPMS and from a different aliquot, 14 spots analyzed by SHRIMP II (Table 2). Only two analyses for each technique show common-Pb contributions above 10%, while 14 and 5 analyses, respectively, exhibit common-Pb below 5%, which is favorable for determination of the intercept with the T–W Concordia curve. An ^{206}Pb/^{238}U intercept age at 2.095 ± 0.038 Ma (MSWD = 0.96) was calculated taking into account 12 out of 14 SHRIMP spot analyses (Fig. 7). Analyses 1.1 and 3.1 have significantly older ages (2.33 and 2.27 Ma) and were rejected. The LA-MC-ICPMS data gives an ^{206}Pb/^{238}U intercept age of 2.129 ± 0.027 Ma (MSWD = 1.90) taking into account 17 of 22 spot analyses (Fig. 8). Five analyses (4.1, 6.1, 13.1, 19.1 and 20.1) again have significantly older ages (2.45, 2.54, 2.46, 2.27 and 2.27 Ma) and were not included in the intercept age calculation. The intercept ages calculated by both techniques are within the analytical errors. The age uncertainties are also very similar. Both sets of analyses show a significant number of older ages: 3 around 2.47 ± 0.04 Ma and 4 around 2.28 ± 0.04 Ma, respectively. Although the aim of this part of our work is not to discuss the geochronological implications of these new zircon ages, older grains (inherited, contamination from the wall rocks, residence time of the magma, etc.) are likely to be present in the Sanadoire phonolite. Returning to the analytical results themselves, it can again be observed that the LA-MC-ICPMS MSWD is slightly higher than expected for a population of 17 analyses: 1.90 instead of 1.73. In comparison, SHRIMP data gave a low MSWD at 0.96. Considering the MSWD for both techniques and the very good quality of the zircon grains, it is probable that the individual errors calculated in the case of LA-MC-ICPMS measurements are slightly underestimated as compared to SHRIMP individual errors.

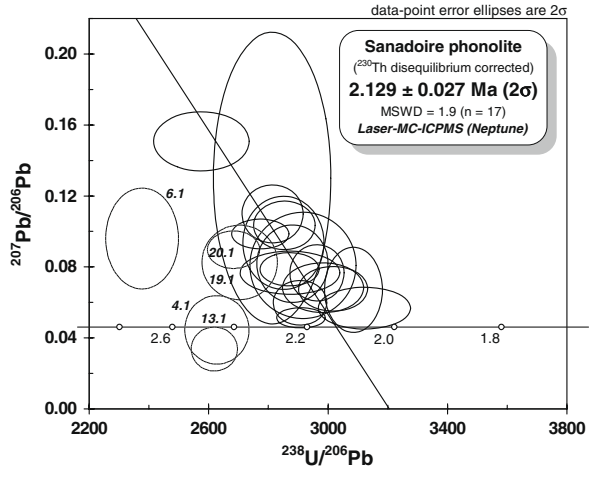

Fig. 8. Age determination for zircon from Sanadoire phonolite using LA-MC-ICPMS (corrected for ^{230}Th disequilibrium and common-Pb).

In conclusion, we have demonstrated using the reference zircon 61.308B and zircon grains from Sanadoire that LA-MC-ICPMS can accurately date very young zircon with adequate precision.

4. RESULTS FOR QUEUREUILH ZIRCONS

The Queureuilh ash and pumice sample is from a trachytic pyroclastic flow (Monts Dore Massif). It is characterized by the presence of bipyramidal zircons not found in the

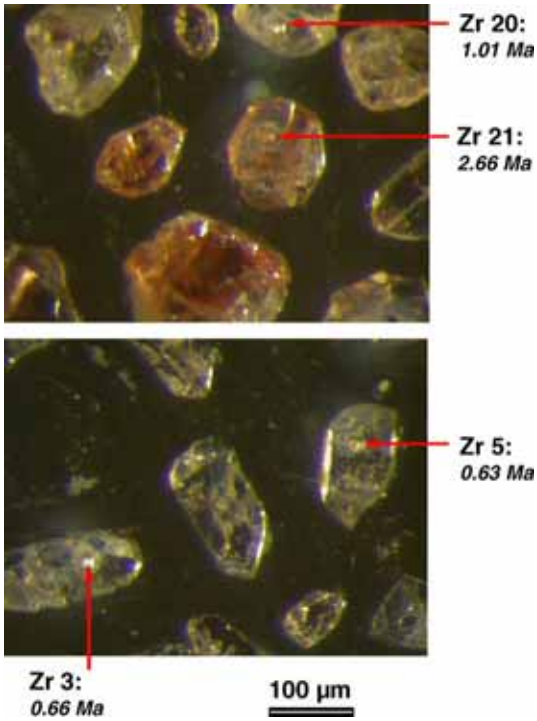

Fig. 9. Post-analysis (LA-MC-ICPMS) photos of representative zircon grains from Queureuilh pumice. The related craters have been marked with a red arrow. Note that the most colored grains show older ages. (For interpretation of the references to color in this figure legend, the reader is referred to the web version of this article.)

Index T \ Index A	100	200	300	400	500	600	700	800
100	B	AB_1	AB_2	AB_3	AB_4	AB_5	A	C
200	H	L_1	L_2	L_3	L_4	L_5	$G_{1\text{-}3}$	I
300	Q_1	S_1	S_2	S_3	S_4 1	S_5	P_1	R_1
400	Q_2	S_6	S_7	S_8 1	S_9	S_{10}	P_2	R_2
500	Q_3	S_{11}	S_{12}	S_{13} 2	S_{14}	S_{15}	P_3	R_3
600	Q_4	S_{16}	S_{17} 2	S_{18} 2	S_{19} 2	S_{20} 1	P_4	R_4
700	Q_5	S_{21} 5	S_{22} 11	S_{23} 11	S_{24} 10	S_{25} 8	P_5 4	R_5
800	E	J_1	J_2	J_3	J_4 2	J_5 2	D 5	F

Fig. 10. Typology of Queureuilh zircons (Pupin, 1980). Most of the grains are of the high temperature type while the colored grains are mainly located on the right of the diagram. The figures in the boxes indicate the number of identified zircon grains of the related type observed from a set of 100 grains.

other pumice flows (Pastre, 1987). This formation has been dated at 0.571 ± 0.060 Ma by K-feldspar $^{40}Ar/^{39}Ar$ analyses (Duffell, 1999). The separated zircon grains are clear and generally well crystallized. They are mainly colorless but some are yellowish to reddish (Fig. 9). Typological study according to the morphology of the grains (Pupin, 1980) shows that colored grains are of the S25, P5, D, J5 and J4 type while colorless or weakly colored grains are represented in the rest of the diagram (Fig. 10). Note that the J and D types are representative of zircon having crystallized at relatively higher temperature. Cathodoluminescence images (Fig. 11) reveal faint and broad zoning.

LA-MC-ICMPS and SHRIMP data are reported in Table 3. Since it has been demonstrated in the previous section that accuracy and precision are similar (see Sanadoire zircon dating), analyses obtained using both techniques can be plotted and interpreted together as a composite sampling. Except for significantly older ages around 2.4 Ma, all other ages range from 1.06 ± 0.03 to 0.54 ± 0.07 Ma showing two main groups of ages around 1.0 and 0.6 Ma. A general observation is that the less colored the grain the younger its age (see Table 3 and Figs. 9 and 11). Because all the analyzed grains are clear and well crystallized and because they are young and contain moderate amounts of U (usually below 1000 ppm), we consider that such grains are likely to retain all radiogenic Pb produced and no radiogenic Pb loss can have occurred during such a short period of time. In other words, they are unlikely to have suffered any radiation damage (Balan et al., 2001). Consequently, all $^{206}Pb/^{238}U$ ages are assumed to be meaningful. Because more than a single event appears to be recorded a procedure to rigorously evaluate the temporal resolution of Queureuilh geochronologic data was applied: the "Mixture Modeling" algorithm of Sambridge and Compston (1994), via ISOPLOT/EX, was used to un-mix statistical age populations or groupings. The resulting curve (Fig. 12) gave

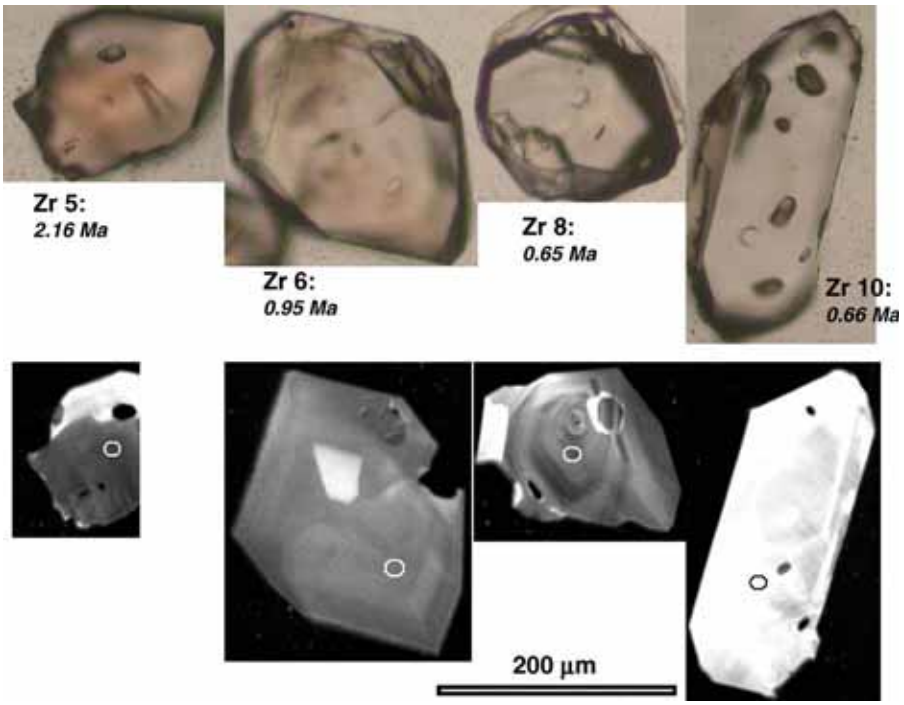

Fig. 11. Representative transmitted light and cathodoluminescence images of zircon grains from Queureuilh pumice analyzed using SHRIMP II. Spots are visible on the post-analysis transmitted light images and are also marked on the CL images. The colorless grains are younger than the colored grains.

Table 3
Summary of SHRIMP and LA-MC-ICPMS U–Pb results for zircon from Queureuil pumice. In *italics*, data not included in the average ages of the zircons.

Grain spot	U (ppm)	Th (ppm)	Th/U	$^{206}Pb^{*}$ (ppm)	$^{206}Pb/^{204}Pb$	f_{206} %	Total (U–Th desequil. corrected)				f Th/U	Radiogenic		Age (Ma)	
							$^{238}U/^{206}Pb$	±	$^{207}Pb/^{206}Pb$	±		$^{206}Pb/^{238}U$	±	$^{206}Pb/^{238}U$	±
LA-MC-ICPMS															
LA-1.1	100	132	1.31	0.008	32	41.90	5903	245	0.3756	0.0156	0.437	0.000098	0.000004	0.634	0.026
LA-2.1	127	188	1.48	0.011	—	17.21	8075	180	0.1814	0.0126	0.493	0.000103	0.000002	0.661	0.015
LA-3.1	399	663	1.66	0.032	—	4.47	9345	148	0.0812	0.0036	0.554	0.000102	0.000002	0.659	0.010
LA-4.1	*127*	*148*	*1.17*	*0.012*	—	—	*7972*	*160*	*0.0364*	*0.0027*	*0.390*	*0.000125*	*0.000003*	*0.809*	*0.016*
LA-5.1	608	1466	2.41	0.051	2269	5.89	9689	111	0.0924	0.0035	0.804	0.000097	0.000001	0.626	0.007
LA-6.1	78	104	1.34	0.006	8	19.59	7929	432	0.2001	0.0236	0.446	0.000101	0.000006	0.654	0.036
LA-7.1	*330*	*487*	*1.48*	*0.029*	*35*	*3.11*	*8455*	*162*	*0.0705*	*0.0042*	*0.492*	*0.000115*	*0.000002*	*0.739*	*0.014*
LA-9.1	*122*	*145*	*1.18*	*0.012*	—	*41.31*	*4771*	*191*	*0.3709*	*0.0135*	*0.394*	*0.000123*	*0.000005*	*0.793*	*0.032*
LA-10.1	70	77	1.11	0.008	—	13.61	5514	137	0.1531	0.0197	0.369	0.000157	0.000004	1.010	0.025
LA-11.1-c	147	230	1.57	0.011	17	7.68	9277	210	0.1064	0.0121	0.522	0.000100	0.000002	0.642	0.014
LA-12.1-c	125	158	1.26	0.038	—	0.44	2728	29	0.0496	0.0038	0.419	0.000365	0.000004	2.352	0.025
LA-13.1-c	341	555	1.63	0.047	—	2.50	5925	80	0.0658	0.0040	0.543	0.000165	0.000002	1.061	0.014
LA-14.1-c	688	1544	2.25	0.092	215	3.64	6213	54	0.0747	0.0023	0.748	0.000155	0.000001	1.000	0.009
LA-15.1-c	127	121	0.96	0.040	278	10.93	2411	34	0.1320	0.0053	0.319	0.000369	0.000005	2.381	0.033
LA-16.1-c	419	452	1.08	0.053	67	15.03	5478	122	0.1642	0.0077	0.360	0.000155	0.000003	1.000	0.022
LA-17.1-c	*242*	*374*	*1.55*	*0.029*	*58*	*9.07*	*6238*	*87*	*0.1174*	*0.0059*	*0.516*	*0.000146*	*0.000002*	*0.940*	*0.013*
LA-18.1-c	680	1778	2.62	0.094	—	1.77	6142	57	0.0600	0.0021	0.872	0.000160	0.000001	1.031	0.010
LA-19.1-c	1199	3414	2.85	0.164	271	2.19	6308	50	0.0633	0.0017	0.949	0.000155	0.000001	0.999	0.008
LA-20.1-c	347	654	1.89	0.045	136	6.46	5969	104	0.0969	0.0057	0.629	0.000157	0.000003	1.010	0.018
LA-21.1-c	*274*	*409*	*1.50*	*0.097*	—	*1.11*	*2400*	*22*	*0.0548*	*0.0020*	*0.498*	*0.000412*	*0.000004*	*2.656*	*0.024*
LA-22.1-c	1728	8958	5.18	0.242	—	0.87	6691	40	0.0529	0.0010	1.728	0.000148	0.000001	0.955	0.006
SHRIMP															
S′-1.1-c	58	36	0.62	0.026	6	34.01	1897	130	0.3147	0.0428	0.206	0.000347	0.000037	2.237	0.237
S″-1.2-c	82	66	0.81	0.031	17	32.90	2218	139	0.3048	0.0397	0.272	0.000303	0.000029	1.950	0.187
S′-2.1-c	1178	4932	4.19	0.179	98	6.11	5888	248	0.0943	0.0082	1.396	0.000159	0.000008	1.027	0.048
S″-2.2-c	927	2331	2.51	0.136	100	7.87	5752	156	0.1079	0.0095	0.838	0.000160	0.000005	1.032	0.031
S′-3.1-c	1689	8497	5.03	0.255	87	3.20	6076	157	0.0713	0.0060	1.676	0.000159	0.000005	1.027	0.032
S″-3.2-c	1653	7666	4.64	0.248	128	4.95	6044	125	0.0850	0.0089	1.546	0.000157	0.000004	1.014	0.027
S′-4.1-c	*183*	*125*	*0.68*	*0.046*	*33*	*7.65*	*3295*	*165*	*0.1065*	*0.0199*	*0.228*	*0.000280*	*0.000015*	*1.806*	*0.097*
S″-4.2-c	197	116	0.59	0.056	93	13.04	2913	116	0.1486	0.0176	0.196	0.000299	0.000013	1.924	0.086
S′-5.1-c	369	432	1.17	0.106	—	2.91	2893	165	0.0691	0.0093	0.390	0.000336	0.000019	2.163	0.120
S″-5.2-c	103	80	0.77	0.039	—	18.38	2233	105	0.1906	0.0259	0.258	0.000366	0.000022	2.356	0.141
S′-6.1-c	250	365	1.46	0.035	19	13.85	5820	356	0.1554	0.0225	0.487	0.000148	0.000010	0.953	0.061
S″-6.2-c	162	182	1.12	0.028	15	29.94	4678	262	0.2815	0.0365	0.373	0.000150	0.000012	0.965	0.079
S′-7.1-c	550	1086	1.98	0.076	49	8.62	5981	219	0.1141	0.0124	0.659	0.000153	0.000006	0.984	0.038
S″-7.2-c	651	1141	1.75	0.096	—	9.38	5590	182	0.1198	0.0129	0.584	0.000162	0.000006	1.045	0.037
S″-7.3-c	*96*	*95*	*1.00*	*0.022*	*11*	*55.46*	*3546*	*217*	*0.4822*	*0.0591*	*0.333*	*0.000126*	*0.000022*	*0.810*	*0.141*
S′-8.1	769	1189	1.55	0.065	—	4.92	9365	414	0.0849	0.0151	0.515	0.000102	0.000004	0.654	0.028
S″-8.2	544	561	1.03	0.052	38	18.51	8223	360	0.1916	0.0211	0.344	0.000099	0.000005	0.639	0.031
S′-9.1-c	486	917	1.89	0.065	—	4.69	6194	259	0.0831	0.0168	0.629	0.000154	0.000007	0.992	0.045
S″-9.2-c	869	1966	2.26	0.132	62	9.38	5522	151	0.1198	0.0094	0.754	0.000164	0.000005	1.058	0.031
S′-10.1	99	89	0.90	0.012	12	33.76	6413	581	0.3126	0.0617	0.298	0.000103	0.000014	0.664	0.091
S″-10.2	75	62	0.84	0.011	—	57.90	5376	495	0.5013	0.0856	0.279	0.000078	0.000020	0.505	0.130
S′-11.1-c	*750*	*1911*	*2.55*	*0.094*	*73*	*7.83*	*6766*	*248*	*0.1079*	*0.0119*	*0.849*	*0.000136*	*0.000005*	*0.878*	*0.035*
S″-11.2-c	983	3204	3.26	0.145	—	4.95	5860	152	0.0850	0.0093	1.087	0.000162	0.000005	1.045	0.031
S′-12.1	607	717	1.18	0.047	69	16.89	9996	527	0.1795	0.0302	0.394	0.000083	0.000005	0.535	0.033
S″-12.2	358	230	0.64	0.036	96	18.11	7691	406	0.1884	0.0302	0.214	0.000106	0.000006	0.686	0.042
S″-12.3	348	304	0.87	0.038	21	35.26	7180	360	0.3233	0.0320	0.292	0.000090	0.000007	0.581	0.042
S′-13.1	64	81	1.26	0.012	12	38.94	4364	400	0.3535	0.0676	0.421	0.000140	0.000023	0.900	0.146
S″-13.2	93	95	1.03	0.020	21	45.72	3831	244	0.4056	0.0529	0.342	0.000142	0.000019	0.913	0.123
S″-15.1-c	661	1169	1.77	0.098	135	8.03	5573	177	0.1092	0.0123	0.590	0.000165	0.000006	1.064	0.036
S″-16.1-c	1040	2886	2.77	0.155	—	7.70	5741	149	0.1066	0.0084	0.925	0.000161	0.000005	1.036	0.029
S″-17.1-c	82	78	0.95	0.022	22	48.60	3061	196	0.4283	0.0550	0.318	0.000168	0.000025	1.082	0.159
S″-17.2-c	1171	2856	2.44	0.173	71	11.02	5696	144	0.1327	0.0088	0.813	0.000156	0.000004	1.007	0.028
S″-18.1	*350*	*263*	*0.75*	*42.5*	—	*0.56*	*7.063*	*0.099*	*0.0720*	*0.0006*	*0.251*	*0.1408*	*0.0020*	*849*	*11*
S″-18.2	215	184	0.86	0.031	10	39.99	5605	302	0.3605	0.0385	0.286	0.000107	0.000010	0.690	0.063

Notes: (1) Uncertainties given at the one s level. (2) Error in 91,500 zircon reference standard is included in the above errors (LA-MC-ICPMS). (3) Errors in Temora reference zircon calibration were 0.55% and 0.32% for the SHRIMP sessions, included in above errors. (4) f_{206}% denotes the percentage of ^{206}Pb that is common-Pb. (5) Correction for common-Pb made using the measured $^{238}U/^{206}Pb$ and $^{207}Pb/^{206}Pb$ ratios. Following Tera and Wasserburg (1972) as outlined in Williams (1998). (6) $f_{Th/U}$ denotes the degree of Th–U fractionation between mineral and magma which is given by $f = (Th/U)_{mineral}/(Th/U)_{magma}$. For this pumice, average Th/U = 3.0. (7) In case of zircon, a correction for deficit in ^{206}Pb is required, due to a deficiency of ^{230}Th (Schärer, 1984). (8) c-marked spots were analyzed from pinky zircon grains. (9) SHRIMP data were recorded during two sessions (2007: S′ and 2008: S″).

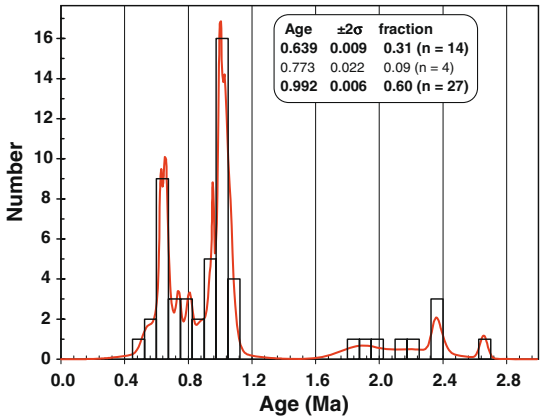

Fig. 12. Histogram plus cumulative plot for Queureuilh ages (individual age uncertainties at 2σ level). The "Unmix Ages" routine from Isoplot allows two main populations to be identified.

two main age groups (at 0.992 ± 0.006 and 0.639 ± 0.009 Ma) accompanied by four intermediate analyses that require specific interpretation. The uncorrected Tera and Wasserburg diagram shows three age groupings (Fig. 13). A group of only red colored grains gives the oldest age of 2.35 ± 0.04 Ma (MSWD = 1.3) considering a group of six analyses. The largest group of data points is for slightly colored grains (see marked analyses in Table 3), with an age of 1.017 ± 0.008 Ma (MSWD = 1.4, 24 analyses). The third population comprises only clear colorless grains, the 14 analyses give an age of 0.640 ± 0.010 Ma (MSWD = 1.4, 14 analyses). Note that the "mixture modeling" routine led to only four analyses being rejected instead of the six analyses as interpreted from the Tera and Wasserburg plot.

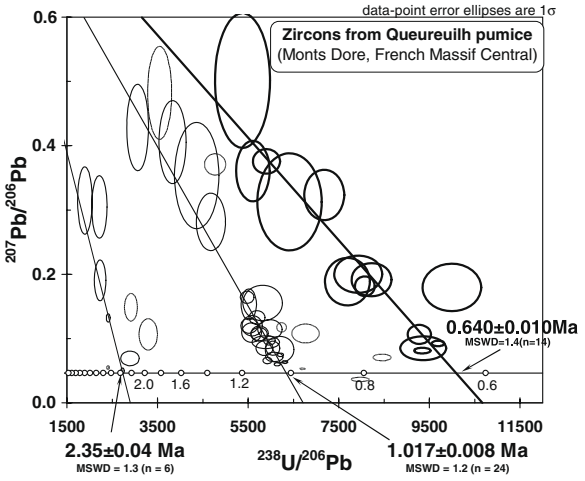

Fig. 13. Age determination for zircons from Queureuilh pumice using SHRIMP II and LA-MC-ICPMS (corrected for ^{230}Th disequilibrium and common-Pb). "Light" ellipses are not taken into account for average age calculations. Note that error ellipses were plotted at 1σ level in order to make easier the reading of the diagram. However, the mean age uncertainties were calculated at 2σ level.

At this time, we prefer to consider the Tera and Wasserburg diagram, as it highlights the level of common-Pb contribution and the error ellipses of the six rejected analyses, ranging from 0.955 ± 0.006 to 0.739 ± 0.014 Ma. In addition, the significantly higher uncertainty calculated in this diagram seems more realistic.

Given the complex nature of the age spectrum a follow-up SHRIMP II session was conducted, in particular to examine the possibility of ~0.64 Ma zircon overgrowing, or rimming the ~1.0 Ma or older zircon. Repeat analyses were carried on 15 grains, with now three analyses on two grains. Despite the use of the CL images, none of the new analyses gave younger ages bordering older areas. There is no evidence of any recrystallization process. However, there is one significant exception: the two analyses of grain #18 document the presence of an 849 ± 11 Ma core to a dominantly 0.69 ± 0.06 Ma zircon grain.

For Queureuilh zircons, the ^{230}Th disequilibrium correction results in an increase of 2.8% of the mean age for the oldest zircons, 2.0% for the 1 Ma population (minimized by high Th/U in zircons) and 5.8% for the youngest group at 0.64 Ma. The Th/U ratio of the magma (3.0) was estimated by measuring Th and U directly in the pumice: 9.3 and 3.1 ppm, respectively. It is obvious that this Th/U ratio is only an estimate in so far as the magma in equilibrium with the various zircon populations is likely to have changed in composition from 2.35 to 0.64 Ma.

Several other comments regarding Th/U, U and Th can also be made. The U content of the dated zircons ranges from 58 to 1728 ppm and the Th/U ratio extends from 0.6 to 5.2. A correlation between such Th–U geochemical data and the calculated ages may be expected. In fact, the oldest grains have a "normal" Th/U ratio of about 1 and the youngest are about 1.3 ± 0.5 (Fig. 14). On the contrary, the grains giving ages around 1 Ma have Th/U ratios always above 1, but with a large variation and a mean value at 2.2 ± 1.1. Some higher values around 5 are also noted (Fig. 14). Potential explanations are: around 1 Ma the mag-

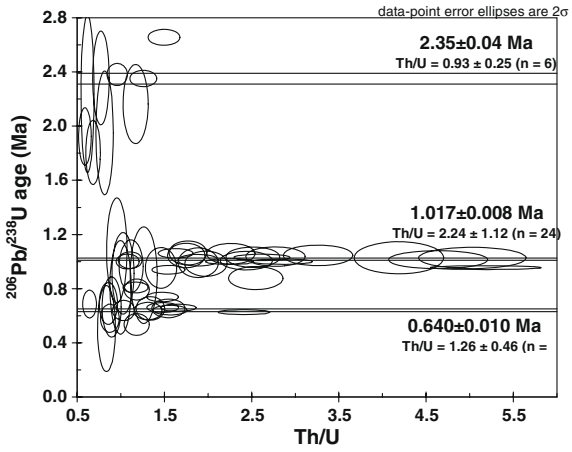

Fig. 14. Age *vs.* Th/U plot for zircon grains from Queureuilh pumice. Note the wide range of variation in the Th/U ratio for zircon grains dated around 1 Ma.

ma chamber was not homogeneous or at that time more than a single magma chamber existed in the crust. Another explanation is that at various times the main magma chamber was intermittently fed by secondary magmas. Our results are similar to those reported by Miller and Wooden (2004), whose zircons appear to have crystallized in contrasting chemical environments. Consequently, the *f* factor is only an estimate because the present day composition of the pumice may not be representative of the Th and U content of the magma at the time when each zircon grain crystallized. However, we observe that the weighted average $^{206}Pb/^{238}U$ ages, corrected for ^{230}Th disequilibrium, are more homogeneous (lower MSWD) than the weighted average uncorrected ages: 1.017 ± 0.008 Ma, MSWD = 1.2 and 1.000 ± 0.013 Ma, MSWD = 2.6 respectively, indicating that our Th/U estimate is probably reasonable. The calculated *f* factors (Table 3) are 0.31 ± 0.08, 0.75 ± 0.37 and 0.42 ± 0.15, respectively, for 2.35 ± 0.04, 1.017 ± 0.008 and 0.640 ± 0.010 Ma old zircons.

5. INTERPRETATION OF THE AGES AND MAGMA RESIDENCE TIME

The first observation considering U–Pb zircon ages and Ar eruption age is that all zircons crystallized prior to eruption and before tephra emplacement. This fact has already been demonstrated by many authors (e.g. Brown and Fletcher, 1999; Farley et al., 2002; Schmitt et al., 2003; etc.). However, magma residence times longer than 1 Myr were considered as not realistic by some authors (Schmitt et al., 2002). However, more recently, Schmitt et al. (2006a) concluded from a detailed study of the Geysers geothermal area (California Coast Ranges) that "two major mantle and crustal reservoirs continually interacted over the 1 Myr duration of volcanism and pluton emplacement at the Geysers. Alternatively, other studies of large plutons have demonstrated an extended history of crystallization up to 5 Myr (Oberli et al., 2004). Similarly, Miller et al. (2007) showed that the time frame of pluton assembly was long: >5 Myr and even >8 Myr for Tuolumne. It is probable that residence time of extensive plutonic magma chambers could be much longer than residence times of small volcanic bodies (Condomines, 1997). Thus, for the Queureuilh pumice, it is highly probable that the rare 2.35 Ma old zircons result from assimilation of local rocks of volcanic origin as suggested by Schmitt et al. (2006b) for a volcano from the Baja California peninsula.

The interpretation of the two younger ages (1.017 and 0.64 Ma) is more problematic. It is especially surprising these two ages are not recorded in a single zircon grain. Only one inherited grain, originated from the base of the crust (849 ± 11 Ma), shows evidence of new zircon growth associated with the latest event (0.69 ± 0.6 Ma). Nevertheless, two main hypotheses are conceivable: (1) there was no input of new magma since 1.017 Ma: the 42 spot ages ranging between 1.017 and 0.64 Ma represent the prolonged evolution of the magma in a closed chamber over 377 kyr. This means that the residence time of the magma in the chamber would last about 446 kyr from 1.017 Ma prior to eruption at 0.571 Ma. (2) The second involves a significant new magma input at 0.64 Ma: the 1.017 Ma zircon crystallization event could correspond to the initial formation of the magma chamber. This age corresponds to the Ar–Ar age of other surrounding lavas of phonolitic composition (Cantagrel and Baubron, 1983). The 0.64 Ma event could be an episodic rejuvenation of the magma, similar to model of Miller and Wooden (2004) for a rhyolitic volcano from California. This model is supported by the contrasting Th/U ratio associated with these two episodes (1.017 and 0.64 Ma). The wide range in Th/U ratios of zircon grains crystallized around 1 Ma suggests a complex history within the age analytical uncertainty: 1.017 ± 0.008 Ma (Fig. 12). During the two main events dated at 1.017 and 0.64 Ma, the almost continuous crystallization of rare zircon grains is interpreted from the presence of analyses ranging from 0.955 and 0.739 Ma (i.e. the six rejected analyses). This model approaches that of Schmitt et al. (2003) which involved zircon recycling by remelting during injection of more mafic magmas. A similar result can be obtained by magma replenishment and mixing with residual phases of older silicic magma chambers (Brown and Fletcher, 1999). Vazquez et al. (2007) have also shown that coeval evolution of chemically distinct magma reservoirs characterized alkalic magma generation in Hawaii. In addition, as concluded by Simon et al. (2007), it is unlikely that volcanism could erupt from a single long-lived magma chamber: rather there would be an episodic record with different magmas. In fact all of these models lead to the same residence time of the magma of about 446 kyr, if we admit that the composition of the magma in the chamber and its location in the crust can change during that time. Nevertheless, the residence time of the magma is much shorter if only the last stage of evolution of the magma is considered when the composition remains constant and the location of the chamber is fixed as a shallow reservoir. The final magma residence would last from the crystallization of the colorless zircon grains at 0.640 Ma until the eruption at 0.571 Ma ($^{40}Ar/^{39}Ar$): i.e. 70 kyr. But the uncertainty as regards this duration is significant as far as the precision on these ages must be considered: ± 0.010 and ± 0.060 Ma, respectively. Finally, considering the two different types of zircon grains (different color: yellowish and colorless), the distinct Th/U ratios and the age discontinuity, it seems that two main age populations represent two discrete zircon crystallization events. The residence time of the final magma in the last reservoir could be ~70 kyr. A first important stage of formation of this magma chamber can take place, perhaps at a deeper level, 377 kyr earlier. This is in agreement with the change in the Th/U ratio from the zircons and lead to a global magma residence time of about 446 kyr.

The study of such Quaternary tephras shows that in a very short period of time (1–2 Myr) several generations of zircon can crystallize and be collected in a single material originated from a complex magma chamber. Zr is mainly present in the studied rocks at stoichiometric proportions in zircon, Zr cannot behave as an incompatible trace element matching Henry's law even if the total amount of Zr is very low in the total rock. In addition, this study shows that the Zr content can be related to various stages of the magma generation and that the volcanic glasses as-

sumed to be representative of the corresponding melt are far from being in equilibrium in each of the zircon grains. This is also stressed by the wide range of Th/U ratios of the analyzed zircons. Thus, the use of Zr concentration in geochemical modeling of whole rock compositional data can be problematic.

6. CONCLUSIONS

Zircons from the Queureuilh Quaternary tephras (pumice) provide new information about the complex history of the magma just before eruption.

1. It is demonstrated that LA-MC-ICPMS applied to U–Pb age determination is an alternative to the SHRIMP method for very young zircons, without complex internal structure.
2. After correction for initial ^{230}Th disequilibrium, the intersection of the common-Pb linear trend with the Tera-Wasserburg Concordia provides reliable ^{206}Pb/^{238}U ages. The underestimate of ^{206}Pb/^{238}U ages uncorrected for ^{230}Th deficit in zircon is 6% for 0.6 Ma old crystals showing a Th/U ratio of 1.5.
3. Zircon grains from the studied pumice flow range over a wide span of time from 2.6 Ma to the age of the eruption, 0.57 Ma (^{40}Ar/^{39}Ar).
4. The discrete age distribution at 2.35 ± 0.04, 1.017 ± 0.008 and 0.640 ± 0.010 Ma allows the evolution of the magma chamber and magma residence to be discussed. The oldest group, less numerous, represents xenocrystic grains resulting from assimilation of local material during magma ascent or eruption. A deep magma chamber formed at 1.01 Ma. The related magma underwent rejuvenation during ascent of the magma in a new chamber at shallow depth and/or during injection of more mafic magmas. During this stage, at 0.64 Ma, the colorless zircon grains crystallized. This stage defines the last stage of evolution of the magma and is interpreted as the magma residence time of 70 kyr prior to eruption (^{40}Ar/^{39}Ar age). According to the definition of "residence time", if the primitive magma is considered, the magma residence time as a whole reaches 446 kyr.
5. This work has shown the difficulty in defining an empirical partition coefficient (Kd_{Zr}) for Zr between any mineral phase and zircon-bearing melt, considering the whole rock as representative of the melt. In addition, in so far as Zr is concentrated in zircon grains of various origin and age, the Zr content must be considered with great care for geochemical purposes and modeling.

ACKNOWLEDGMENTS

We thank N. Arnaud and P. Rossi for helpful discussions. We are also indebted to C. Bény for back scattered electron images of laser craters. We thank C.R. Bacon and an anonymous reviewer for constructive comments and especially F. Oberli for detailed comments that improved the manuscript. The work for this BRGM contribution No. 05762 was supported by a BRGM research grant.

REFERENCES

Alloway B. V., Larsen G., Lowe D. J., Shane P. A. R. and Westgate J. A. (2006) Tephrochronology. In *Encyclopaedia of Quaternary Science* (ed. S. A. Elias). Elsevier, London, pp. 2869–2898.

Bachmann O., Oberli F., Dungan M. A., Meier M., Mundil R. and Fischer H. (2007a) ^{40}Ar/^{39}Ar and U–Pb dating of fish canyon magmatic system, San Juan volcanic field, colorado: evidence for an extended crystallization history. *Chem. Geol.* **236**, 134–166.

Bachmann O., Charlier B. L. A. and Lowenstern J. B. (2007b) Zircon crystallization and recycling in the magma chamber of the rhyolitic Kos Plateau Tuff (Aegean arc). *Geology* **35**, 73–76.

Bacon C. R. and Lowenstern J. B. (2005) Late Pleistocene granodiorite source for recycled zircon and phenocrysts in rhyodacite lava at Crater Lake, Oregon. *Earth Planet. Sci. Lett.* **233**, 277–293.

Bacon C. R., Persing H. M., Wooden J. L. and Ireland T. R. (2000) Late Pleistocene granodiorite beneath Crater Lake caldera, Oregon, dated by ion microprobe. *Geology* **28**, 467–470.

Balan E., Neuville D. R., Trocellier P., Fritsch E., Muller J.-P. and Calas G. (2001) Metamictization and chemical durability of detrital zircon. *Amer. Mineral.* **86**, 1025–1033.

Baubron J. C. and Cantagrel J. M. (1980) Les deux volcans des Monts Dore (Massif Central français): arguments chronologiques. *C. R. Acad. Sci. Paris* **290**, 1409–1412.

Black L. P., Kamo S. L., Allen C. M., Aleinikoff J. N., Davis D. W., Korsch R. J. and Foudoulis C. (2003) TEMORA 1: a new zircon standard for phanerozoic U–Pb geochronology. *Chem. Geol.* **200**, 155–170.

Brown S. J. A. and Fletcher I. R. (1999) SHRIMP U–Pb dating of preeruption growth history of zircons from the 340 Ka Whakamaru Ignimbrite, New Zealand: evidence for >250 ky magma residence times. *Geology* **27**, 1035–1038.

Cantagrel J. M. and Baubron J. C. (1983) Chronologie des éruptions dans le massif volcanique des Monts Dore (méthode potassium–argon) implications volcanologiques. *Géol. Fr.* **1**, 123–142.

Cherniak D. J. and Watson E. B. (2000) Pb diffusion in zircon. *Chem. Geol.* **172**, 5–24.

Claoué-Long J. C., Compston W., Roberts J. and Fanning C. M. (1995) Two Carboniferous ages: a comparison of SHRIMP zircon dating with conventional zircon ages and^{40} Ar/^{39} Ar analysis. Geochronology Time Scales and Global Stratigraphic Correlation. SEPM Special Publication **54**, pp. 1–21.

Cocherie A., Fanning C. M., Jezequel P. and Robert M. (2007) LA-MC-ICPMS applied for in situ U–Pb dating of 2 Ma zircons using a multi-ion counting system. In "Accessory minerals in-situ: microanalytical methods and petrological applications", Krakow, 15–16th September 2007. *Mineral. Pol.* **30**, 61–63.

Cocherie A. and Robert M. (2007) Direct measurement of lead isotope ratios in low concentration environmental samples by MC-ICPMS and multi-ion counting. *Chem. Geol.* **243**, 90–104.

Cocherie A. and Robert M. (2008) Laser ablation coupled with ICP-MS applied to U–Pb zircon geochronology: a review of recent advances. *Gondwana Res.* **14**, 597–608.

Compston W. (1999) Geological age by instrumental analysis: the 29th Hallimond Lecture. *Mineral. Mag.* **63**, 297–311.

Compston W., Williams I. S. and Clement S.W. (1982) U–Pb ages within single zircons using a sensitive high mass-resolution ion microprobe. *Amer. Soc. Mass Spect. Conf.,* 30th, Honolulu, pp. 593–595.

Condomines M. (1997) Dating recent volcanic rocks through ^{230}Th–^{238}U disequilibrium in accessory minerals: example of the Puy de Dôme (French Massif Central). *Geology* **25**, 375–378.

Cumming G. L. and Richards J. R. (1975) Ore lead isotope ratios in a continually changing Earth. *Earth Planet. Sci. Lett.* **28**, 155–171.

Duffell H. (1999) Contribution géochronologique à la stratigraphie volcanique du Massif des Monts Dore par la méthode $^{40}Ar/^{39}Ar$. D.E.A. Univ. Clermont-Ferrand, 56 p.

Farley K. A., Kohn B. P. and Pillans B. (2002) The effects of secular disequilibrium on (U–Th)/He systematics and dating of Quaternary volcanic zircon and apatite. *Earth Planet. Sci. Lett.* **201**, 117–125.

Hervig R. L., Mazdab F. K., Williams P., Guan Y., Huss G. R. and Leshin L. A. (2006) Useful ion yields for Cameca IMS 3f and 6f SIMS: limits on quantitative analysis. *Chem. Geol.* **227**, 83–99.

Hirata T. (1997) Soft ablation technique for laser ablation-inductively coupled plasma mass spectrometry. *J. Anal. Atom. Spectrom.* **12**, 1337–1342.

Hirata T., Iizuka T. and Orihashi Y. (2005) Reduction of mercury background on ICP-mass spectrometry for in situ U–Pb age determinations of zircon samples. *J. Anal. Atom. Spectrom.* **20**, 696–701.

Horstwood M. S. A., Foster G. L., Parrish R. R., Noble S. R. and Nowell G. N. (2003) Common-Pb corrected in situ U–Pb accessory mineral geochronology by LA-MC-ICP-MS. *J. Anal. Atom. Spectrom.* **18**, 837–846.

Ludwig K. R. (2001) *SQUID 1.02, A user's Manual*. Berkeley Geochronology Center, Spec. Pub. No. 2.

Ludwig K. R. (2003) *Isoplot/EX, version 3. A geochronological toolkit for Microsoft Excel*. Berkeley Geochronology Center, Spec. Pub. No. 4, 70 p.

Miller J. S. and Wooden J. L. (2004) Residence, resorption and recycling of zircons in Devils Kitchen rhyolite, Coso volcanic field, California. *J. Petrol.* **45**, 2155–2170.

Miller J. S., Matzel J. E. P., Miller C. F., Burgess S. D. and Miller R. B. (2007) Zircon growth and recycling during the assembly of large, composite arc plutons. *J. Volcanol. Geotherm. Res.* **167**, 282–299.

Oberli F., Meier M., Berger A., Rosenberg C. L. and Gieré R. (2004) U–Th–Pb and $^{230}Th/^{238}U$ disequilibrium isotope systematics: precise accessory mineral chronology and melt evolution tracing in the Alpine Bergell intrusion. *Geochim. Cosmochim. Acta* **68**, 2543–2560.

Palfy J., Mundil R., Renne P. R., Bernor R. L., Kordos L. and Gasparik M. (2007) U–Pb and $^{40}Ar/^{39}Ar$ dating of the Miocene fossil track site at Ipolytarnoc (Hungary) and its implications. *Earth Planet. Sci. Lett.* **258**, 160–174.

Pastre J. F. (1987) Les formations Plio-quaternaires du Bassin de l'Allier et le volcanisme régional (massif Central, France). Rapports géodynamiques et stratigraphiques, corrélations téphrochronologiques, implications. Ph.D. Thesis, Univ. Paris VI. 733p.

Paul B., Woodhead J. D. and Hergt J. (2005) Improved in situ isotope analysis of low-Pb materials using LA-MC-ICP-MS with parallel ion counter and Faraday detection. *J. Anal. Atom. Spectrom.* **20**, 1250–1357.

Pupin J. P. (1980) Zircon and granite petrology. *Contrib. Mineral Petrol* **73**, 207–220.

Sambridge M. S. and Compston W. (1994) Mixture modeling of multi-component data sets with application to ion-probe zircon ages. *Earth Planet. Sci. Lett.* **128**, 373–390.

Schärer U. (1984) The effect of initial ^{230}Th disequilibrium on young U–Pb ages: the Makalu case, Himalaya. *Earth Planet. Sci. Lett.* **67**, 191–204.

Schmitt A. K., Grove M., Harrison M., Lovera O., Hulen J. and Walters M. (2003) The Geysers–Cobb Montain Magma System, California (Part 1): U–Pb zircon ages of volcanic rocks, conditions of zircon crystallization and magma residence times. *Geochim. Cosmochim. Acta* **67**, 3423–3442.

Schmitt A. K., Lindsay J. M., de Silva S. and Trumbull R. B. (2002) U–Pb zircon chronostratigraphy of early-Pliocene ignimbrites from La Pacana, north Chile: implications for the formation of stratified magma chambers. *J. Volcanol. Geotherm. Res.* **120**, 43–53.

Schmitt A. K., Romer R. L. and Stimac J. A. (2006a) Geochemistry of volcanic rocks from the Geysers geothermal area, California Coast Ranges. *Lithos* **87**, 80–103.

Schmitt A. K., Stockli D. F. and Hausback B. P. (2006b) Eruption and magma crystallization ages of Las Tres Virgenes (Baja California) constrained by combined $^{230}Th/^{238}U$ and (U–Th)/He dating of zircon. *J. Volcanol. Geotherm. Res.* **158**, 281–295.

Simon J. I., Reid M. R. and Young E. D. (2007) Lead isotopes by LA-MC-ICPMS: tracking the emergence of mantle signatures in an evolving silicic magma system. *Geochim. Cosmochim. Acta* **71**, 2014–2035.

Simon J. I., Renne P. R. and Mundil R. (2008) Implication of pre-eruptive magmatic histories of zircons for U–Pb geochronology of silicic extrusions. *Earth Planet. Sci. Lett.* **266**, 182–194.

Simonetti A., Heaman L. M., Hartlaub R. P., Creaser R. A., MacHattie T. G. and Böhm C. (2005) U–Pb zircon dating by laser ablation-MC-ICP-MS using a new multiple ion counting Faraday collector array. *J. Anal. Atom. Spectrom.* **20**, 677–686.

Tera F. and Wasserburg G. J. (1972) U–Th–Pb systematics in three Apollo 14 basalts and the problem of initial Pb in lunar rocks. *Earth Planet. Sci. Lett.* **14**, 281–304.

Tiepolo M. (2003) In situ Pb geochronology of zircon with laser ablation-inductively coupled plasma-sector field mass spectrometry. *Chem. Geol.* **199**, 159–177.

Vazquez J. A., Shamberger P. J. and Hammer J. E. (2007) Plutonic xenoliths reveal the timing of magma evolution at Hualalai and Mauna Kea, Hawaii. *Geology* **35**, 695–698.

Wendt I. and Carl C. (1991) The statistical distribution of the mean squared weighted deviation. *Chem. Geol.* **86**, 275–285.

Wiedenbeck M., Allé P., Corfu F., Griffin W. L., Meier M., Oberli F., von Quadt A., Roddick J. C. and Spiegel W. (1995) Three natural zircon standards for U–Th–Pb, Lu–Hf, trace element and REE analysis. *Geostand. Newslett.* **19**, 1–23.

Williams I. S. (1998) U–Th–Pb geochronology by ion microprobe. *Rev. Ecol. Geol.* **7**, 1–35.

Willigers B. J. A., Baker J. A., Krogstad E. J. and Peate D. W. (2002) Precise and accurate in situ Pb–Pb dating of apatite, monazite, and sphene by laser ablation multiple-collector ICP-MS. *Geochim. Cosmochim. Acta* **66**, 1051–1066.

Associate editor: Alan D. Brandon